PCCP

PAPER

View Article Online
View Journal | View Issue

Cite this: *Phys. Chem. Chem. Phys.*, 2016, **18**, 33031

The intrinsic strength of the halogen bond: electrostatic and covalent contributions described by coupled cluster theory†

Vytor Oliveira, Elfi Kraka and Dieter Cremer*

Received 27th September 2016,
Accepted 17th November 2016

DOI: 10.1039/c6cp06613e

www.rsc.org/pccp

36 halogen-bonded complexes YX···AR_m (X: F, Cl, Br; Y: donor group; AR_m acceptor group) have been investigated at the CCSD(T)/aug-cc-pVTZ level of theory. Binding energies, geometries, NBO charges, charge transfer, dipole moments, electrostatic potential, electron and energy density distributions, difference density distributions, vibrational frequencies, local stretching and bending force constants, and relative bond strength orders *n* have been calculated and used to order the halogen bonds according to their intrinsic strength. Halogen bonding is found to arise from electrostatic and strong covalent contributions. It can be strengthened by H-bonding or lone pair delocalization. The covalent character of a halogen bond increases in the way 3c-4e (three-center-four-electron) bonding becomes possible. One can characterize halogen bonds by their percentage of 3c-4e bonding. FCl–phosphine complexes can form relatively strong halogen bonds provided electronegative substituents increase the covalent contributions in form of 3c-4e halogen bonding. Binding energies between 1 and 45 kcal mol^{-1} are calculated, which reflects the large variety in halogen bonding.

1 Introduction

Halogen bonding (XB; in the following also used for halogen bond and halogen-bonded) is a non-covalent interaction formed between an electrophilic halogen atom X in XY (dihalogens, interhalogens; or halogenated molecules) and a nucleophilic heteroatom A (*i.e.* A with lone-pair (lp) electrons) where XB can take place in the gas phase, solution, or the solid state. Due to its unique features, XB is increasingly used in medicinal,[1–3] supramolecular, and materials chemistry,[4–10] apart from its role in structural chemistry,[11–14] synthesis[8,15,16] or catalysis.[14,16,17] Therefore, XB has been the topic of several recent reviews.[2,5,10,13,16,18–22] In this connection, the excellent review by Metrangolo and co-workers[10] and the earlier work of these authors on XB[23–25] deserves special attention. XB was already observed 200 years ago[10] and ever since played some role in synthetic chemistry.[10] However, its nature was only understood in the last two decades when quantum chemical studies focused on XB.[20,26–36] It became soon clear that high-accuracy quantum chemical methods are needed to reliably describe XB, especially when involving fluorine. Nevertheless, the number of high accuracy studies on XB is still limited.[33–40]

Karpfen[36] analyzed XBs between X_2 or XY (F_2, Cl_2, Br_2, ClF, BrCl) and NH_3 utilizing CCSD(T). He found that binding energies do not follow the trends in the XY dipole moments or XY polarizabilities. Legon[33] and Hill and Hu[35] performed CCSD(T)-F12 calculations pointing out the relationship between various complex properties and the complex binding energy. Hiberty and co-workers[37] compared the bonding features of trihalides X_3^- (X = F, Cl, Br, I) utilizing valence bond and CCSD(T) theory. Other authors carried out benchmark calculations on neutral and charged XB-complexes at the CCSD(T)/CBS (complete basis set limit) level to obtain reliable XB distances, binding energies and interaction energies (complex binding energies for frozen geometries of the monomers).[32,34,38,41]

Other quantum chemical investigations on XB were based on less accurate methods such as DFT (density functional theory),[38,41–48] or second order Møller–Plesset perturbation theory.[12,49–59] Symmetry-adapted perturbation theory[15,51,57,60–64] or other energy decomposition methods[52,54,64] were used to partition the XB binding energy into electrostatic, exchange, dispersion, *etc.* contributions. Since the nature of XB is reflected by the charges of the atoms involved (A and X), the charge transfer from R_mA to XY, charge polarization of the monomers, the electron density distribution $\rho(\mathbf{r})$, its Laplacian, the energy density distribution $H(\mathbf{r})$, or the electrostatic potential $V(\mathbf{r})$ were analyzed.[44,50,51,53,55,62,65–74]

Computational and Theoretical Chemistry Group (CATCO), Department of Chemistry, Southern Methodist University, 3215 Daniel Ave, Dallas, Texas 75275-0314, USA. E-mail: dcremer@smu.edu

† Electronic supplementary information (ESI) available: It contains calculated geometries and energies for all molecules calculated in this work (PDF). Also, NBO charges, dipole moments and polarizabilities of the monomers, the correlation of the intrinsic XB strength with binding energies, bond lengths and density values is shown. See DOI: 10.1039/c6cp06613e

XB should lead to a change in the covalent bond XY. Jemmis[75,76] analyzed changes in the XY distances to explained red/blue-shifted XB-complexes. XY elongation occurs due to the lone pairs of the acceptor atom lp(A) been donated to the antibonding orbital σ*(XY), whereas XY shortening occurs due to a negative hyperconjugation mechanism. Del Bene and co-workers have investigated the spin–spin coupling constants affected by XB.[49,56,77]

A comparison of XB with other non-covalent interactions was carried out by several authors.[12,46,78–83] For example, Mo and co-workers[82] used BLWs (Block-Localized Wavefunctions) to analyze the directionality of non-covalent interactions for halogen, pnicogen, and chalcogen bonding. Scheiner,[80] as well as Elguero and co-workers,[78] reviewed the similarities and differences between halogen, chalcogen, pnicogen, and hydrogen bonding. Grabowski[79] compared the mechanism of hydrogen with halogen bonding.

XB is characterized by three common features: (i) the distance X···A between halogen X and nucleophile (Lewis base) A is shorter than the sum of the van der Waals radii. (ii) The covalent XY distance in the XB complex tends to be longer than in the monomer XY (for exceptions, see Section 3). (iii) The angle YXA is close to 180°.[10] These structural features are electronically related to an interplay of electrostatic and covalent interactions, which results in the strength, tunability, and amphoteric character of XB. The anisotropy of the electron density distribution at X in a singly bonded X–Y causes unique electrostatic features as reflected by a σ-hole (positive electrostatic potential V in the non-bonded direction)[84–86] that is surrounded in the π-direction by a belt of negative charge (negative V). For a σ-hole, the electron density distribution is tightly bonded to the nucleus X so that a nucleophile A with an into space extending lp can dock with the tail density of the lp into the σ-hole of halogen X.[84–86] The σ-hole and the electrostatic attraction should increase with the atomic number of X in the series F < Cl < Br < I < At where F_2 should be the weakest halogen donor in complexes XX···AR_m.[10] π-Systems such as benzene can also function as a Lewis base (instead of a heteroatom) and interact with an electrophilic halogen *via* XB.[10,87,88]

Despite the many investigations of XB carried out so far, there is no quantitative assessment of the XB bond strength. Complex binding energies and interaction energies can provide only a qualitative insight as they include, besides the intrinsic XB strength, all changes in the monomers upon dissociation of a XB dimer. A quantitative and reliable strength parameter is the local XB stretching force constant k^a that probes the intrinsic strength of the XB without changing the electronic structure of the complex as the force constant always refers to an infinitesimally small change in the complex geometry.[89] In general, a stretching force constant (derived, *e.g.*, from the normal mode frequencies or directly from the Hessian of the energy) cannot be used for this purpose as it is always contaminated by mode–mode coupling.[89–91] However, force constants of the local vibrational modes, which are derived from the mass-decoupled Wilson equation[91,92] of vibrational spectroscopy, are no longer flawed by mode–mode coupling and provide a reliable measure of the intrinsic bond strength.[89,93–96] Using local vibrational modes calculated with CCSD(T)[97] as an accurate quantum chemical tool, we will for the first time provide reliable data on the intrinsic strength of XB. In this connection, we will pursue the following objectives and provide answers to the following questions.

(i) The intrinsic bond strength of XB varies. How large can this variation be and how does it depend on donor and acceptor of the XB complex? (ii) What bonding mechanism is responsible for the strength XB? When do electrostatic and when do covalent interactions dominate the bonding mechanism? Can the σ-hole attraction mechanism rationalize the intrinsic strength of XB? (iii) Is the XY bond strength related to the XB strength so that the latter can be anticipated by the former? (iv) Does the YXA bending force constant reflect the XB strength? (v) How does the negative charge of an anion change the strength of a XB? (vi) In the case of the trihalides $[Y\cdots X\cdots Y]^-$ (X, Y: halogen), one obtains ions, which are valence isoelectronic with XeF_2 and, therefore should be characterized by 3c-4e (3-center-4-electron) bonding. These ions should represent systems with covalent XBs. How can one quantify the covalent character of these bonds and the 3c-4e bonding mechanism?

These questions will be answered by investigating 36 neutral and anionic halogen bonded complexes as well as eight complexes with hydrogen, pnicogen, or chalcogen bonding (Fig. 1). Apart from presenting an order of XB according to its intrinsic strength, we will analyze the strength of the XB using two models. The first is based on orbital theory and the second on electron density theory. Whenever one uses a model one has to point out its limitations in connection to the five basic interactions determining the strength of XB: exchange repulsion, covalent, electrostatic, inductive, and dispersion interactions. Recently, Politzer and co-workers[98–100] have put forward the idea that non-covalent interactions such as XB might be described purely on the basis of Coulomb interactions, which have a physical basis. However, to learn about the mechanistic details of non-covalent interactions it is useful to refer to quantum chemical models. In this sense, we will use orbital theory to describe the covalent interactions between the monomers and single out the charge transfer between specific orbitals of the monomers as a reflection of these covalent interactions although part of this charge transfer can be due to other than covalent interactions. In a similar way, we will use the energy density to distinguish between covalent and electrostatic interactions where the former will include all interactions leading to stabilization and a negative energy density whereas the latter lead to destabilization and a positive energy density.

The results of this investigation will be presented in the following way. In Section 2, we will shortly describe the quantum chemical methods and tools used in this work. The nature of the XB will be discussed in Section 3 where the focus is on the role of the XB donor and acceptor. Also, we will investigate the influence of the charge in anionic XB complexes and

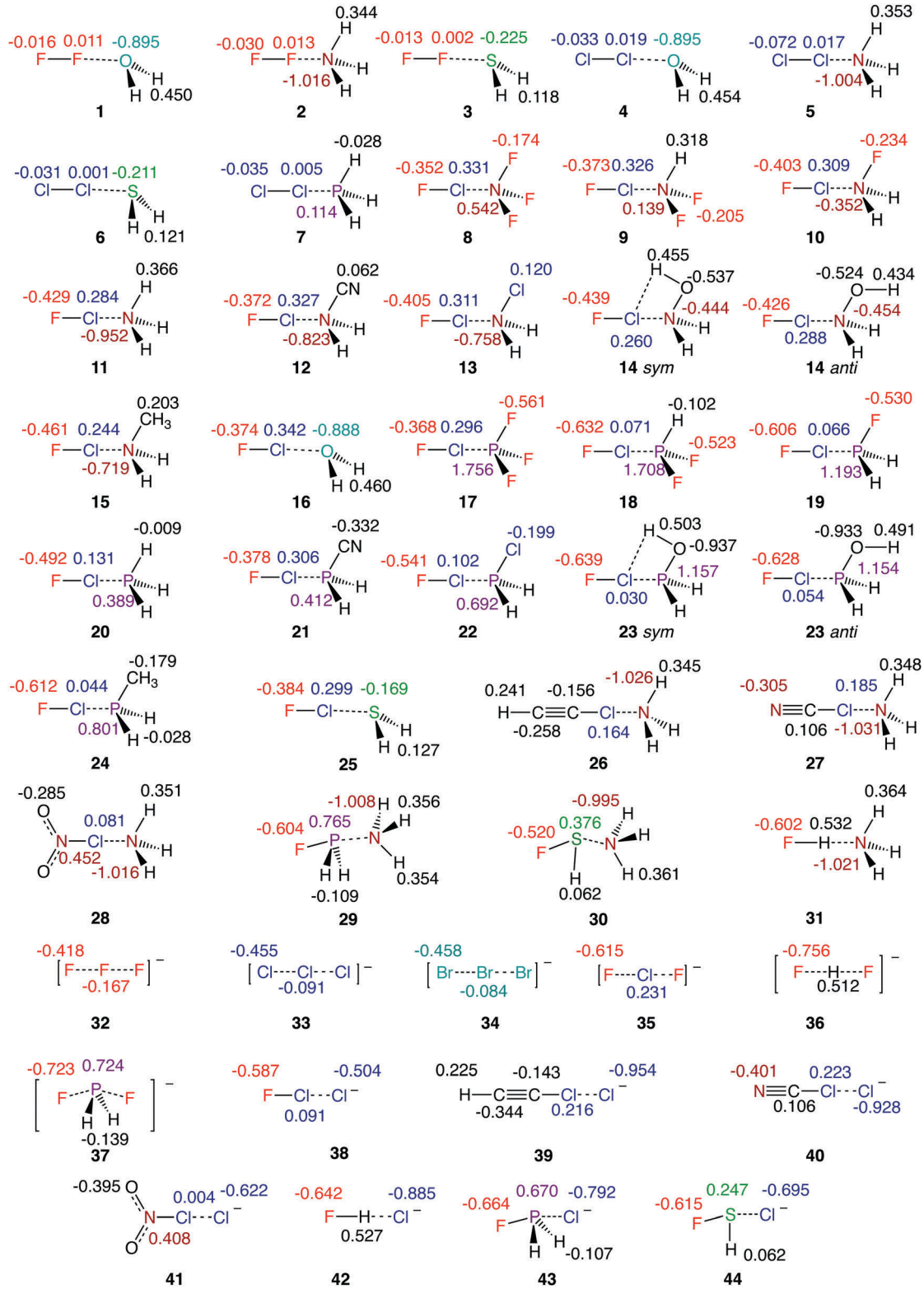

Fig. 1 Schematic representation of complexes **1–44** with selected NBO atomic charges calculated at CCSD(T)/aug-cc-pVTZ. Color is used to relate charges to atoms.

compare XB with other non-covalent bonds. In Section 4, we will analyze how different XB properties commonly used in the literature reflect the strength of XB. Finally, in Section 5, we will draw the conclusions of this investigation and provide an outlook on how the results of this work can be used in the future.

2 Computational methods

The geometries of all complexes investigated were fully optimized at the coupled cluster level using CCSD(T) (all single, double, and perturbative triple excitations are included)[97] and augmented triple zeta basis sets aug-cc-pVTZ,[101–103] which contain diffuse basis functions to describe the charge distribution of heteroatoms or anions and the dispersion interactions in non-covalently bonded complexes. For the geometry optimizations, a convergence criterion of 10^{-7} Hartree Bohr^{-1} was used and for the SCF (self-consistent field) iterations and the iterations of the CC amplitudes a threshold of 10^{-9}.

Each stationary point obtained in the geometry optimizations was identified as a minimum with the help of the analytical frequencies. The normal modes obtained by solving the Wilson equation[92] were used to calculate the local stretching modes and their properties according to the procedures described by Konkoli and Cremer.[89–91,93] Apart from this, all normal modes calculated were characterized in terms of local modes to identify those with strong XB stretching or bending character.[104]

There is a one to one relationship between normal and local vibrational modes,[93] which implies that there are just six local intermonomer vibrations. One of them is the local XB stretching mode characterized by the local stretching frequency ω^a(XB) and the local stretching force constant k^a(XB). As was demonstrated by Zou and Cremer, there is a direct relationship between the local stretching force constant of a bond and its intrinsic strength.[105] Accordingly, the intrinsic strength of the XB was determined by its k^a(XB) value the analysis of which was simplified by converting local stretching force constants into bond strength orders (BSOs) n(XB) according to

$$n = a(k^a)^b \quad (1)$$

with $a = 0.418$ and $b = 0.564$. Eqn (1) is based on the generalized Badger rule derived by Cremer and co-workers.[96,106] Constants a and b were determined by assuming an n value of 1.00 for the FF bond in F_2 and $n = 0.50$ for the 3c-4e bond in $[F\cdots F\cdots F]^-$, which according to the Rundle–Pimentel model of bonding has two electrons in a bonding and two electrons in a non-bonding orbital. For $k^a = 0$, an n value of zero was enforced.

Binding energies ΔE were calculated at the CCSD(T) level after applying the counterpoise correction of Boys and Bernardi[107] to determine the corrections for the basis set superposition errors (BSSE). The atomic charges and the charge transfer between the monomers were calculated with the help of the NBO (natural bond orbital) population analysis[108] using CCSD(T) response densities. Local properties of the electron density distribution, $\rho(\mathbf{r})$, and energy density distribution, $H(\mathbf{r})$, were also computed at the CCSD(T) level of theory. The Cremer–Kraka criteria for covalent bonding were applied.[109–111] These associate a stabilizing energy density at the bond critical point $\mathbf{r}_b$ ($H(\mathbf{r}_b) = H_b < 0$) with dominating covalent character, whereas a destabilizing energy density ($H_b > 0$) indicates bonding due to electrostatic interactions. The electrostatic character of the interactions was also investigated by using the maximum value of the electrostatic potential $V(\mathbf{r})$ on the van der Waals surface (modeled by the 0.001 e Bohr^{-3} electron density surface) of the halogen donor monomers. The halogen acceptor ability of a monomer AR_m was assessed by calculating the most negative value of $V(\mathbf{r})$ in the lp(A) region (Table 2).

Beside calculating the charge transfer between the interacting monomers, we also calculated the difference density distribution $\Delta\rho(\mathbf{r}) = \rho(\text{Complex},\mathbf{r}) - \rho(\text{Monomer1},\mathbf{r}) - \rho(\text{Monomer2},\mathbf{r})$, which was determined and plotted for the complex enveloping surface of an electron density distribution of 0.001 e Bohr^{-3}. A positive difference density in the XB region is an alternative measure for its covalent character.

All local mode calculations were performed with COLOGNE-2016.[112] The CCSD(T) energy, energy gradient, and Hessian were calculated with CFOUR.[113] For the NBO analysis, NBO 6[108] was used whereas the electron (energy) density distribution was investigated with the program AIMAll.[114] Correlated electron and energy density distributions were analyzed with the programs Molden2AIM, and MOLBO of Zou and co-workers.[115] The CCSD(T) electrostatic potential $V(\mathbf{r})$ were calculated with Multiwfn.[116]

3 Results and discussion

Table 1 lists the distances r(XY) between the halogen atom X and the donor group or atom Y, the XB distance r(XA) between X and heteroatom A of the acceptor of the XB, the counterpoise corrected binding energy ΔE, the electron density ρ_b and the energy density H_b at the density critical point associated with XB, the intermonomer charge transfer obtained from the NBO analysis, the local bending force constant k^a(YXA), the local stretching force constant k^a(XY), the percentage of 3c-4e XB given by the ratio n(AX)/n(XY), the local stretching force constant k^a(XA), the BSO n of the XB, and the local frequency ω^a(XA). The last column shows the frequency, the normal mode number m and the percentage of XB stretching character contained in mode m. Calculated NBO atomic charges are given in Fig. 1. Additional properties (dipole moments, static polarizabilities, *etc.*) are given in the ESI.†

In Table 2, the CCSD(T) values of the electrostatic potential, which are used to characterize either the σ-hole or the lp(A) of the monomers are summarized. The BSO values of the XB of all complexes investigated are given as a function of the local X···A stretching force constant in Fig. 2.

In previous work, experimentalist used the halogen stretching force constant as a measure for the intrinsic strength of the XB. Legon and co-workers[33] measured the rotational spectra and the centrifugal constants of XB complexes to determine the intermonomer stretching force constant k_σ, which differs from the local XB stretching force constant k^a(XB) because the former is contaminated by coupling effects with other vibrational modes. Since the coupling effects are small in the case of a complex, one can expect that k_σ values are related to the k^a(XA) values. This expectation is confirmed by the data points of ten representative complexes shown in Fig. 3.

The nature of halogen bonding

There is a covalent and an electrostatic contribution to XB.[10] The covalent contribution is the result of a charge transfer from

Table 1 Geometry, energy, electron density, energy density, and vibrational data for complexes **1–44**[a]

#	Complexes (*sym.*)	r (XY)	r (XA)	ΔE	ρ_b	H_b	CT	k^a (YXA)	k^a (XY)	n (XY)	k^a (XA)	n (XA)	3c-4e (%)	ω^a (XA)	ω_μ (%ω^a)
Dihalogens															
1	$F_2\cdots OH_2$ (C_s)	1.423	2.662	1.15	0.010	0.003	0.005	0.027	4.488	0.974	0.057	0.083	9	105	88(3;99.2)
2	$F_2\cdots NH_3$ (C_{3v})	1.432	2.615	1.69	0.014	0.004	0.017	0.051	3.821	0.890	0.062	0.087	10	114	96(3;100)
3	$F_2\cdots SH_2$ (C_s)	1.425	3.092	0.89	0.008	0.002	0.011	0.027	4.238	0.943	0.034	0.062	7	70	58(3;99.3)
4	$Cl_2\cdots OH_2$ (C_s)	2.027	2.808	2.62	0.015	0.003	0.014	0.088	2.896	0.761	0.097	0.112	15	123	107(3;99.7)
5	$Cl_2\cdots NH_3$ (C_{3v})	2.047	2.664	4.43	0.025	0.001	0.055	0.165	2.370	0.680	0.132	0.133	20	150	131(3;100)
6	$Cl_2\cdots SH_2$ (C_s)	2.032	3.209	2.23	0.013	0.001	0.030	0.078	2.715	0.734	0.069	0.092	13	84	73(3;100)
7	$Cl_2\cdots PH_3$ (C_{3v})	2.034	3.220	2.22	0.014	0.001	0.030	0.064	2.612	0.718	0.062	0.087	12	80	69(3;100)
Interhalogen FCl															
8	$FCl\cdots NF_3$ (C_{3v})	1.650	2.784	1.41	0.017	0.002	0.021	0.076	4.220	0.941	0.081	0.101	11	117	66(3;100)
9	$FCl\cdots NHF_2$ (C_s)	1.660	2.575	3.47	0.028	0.001	0.047	0.166	3.865	0.896	0.131	0.133	15	149	62(2;3.4) 108(3;95.7)
10	$FCl\cdots NH_2F$ (C_s)	1.680	2.400	6.22	0.044	−0.004	0.094	0.279	3.156	0.799	0.197	0.167	21	183	149(2;98.9)
11	$FCl\cdots NH_3$ (C_{3v})	1.703	2.320	9.39	0.053	−0.009	0.145	0.434	2.687	0.729	0.311	0.216	30	230	207(3;100)
12	$FCl\cdots NH_2CN$ (C_s)	1.662	2.594	3.88	0.028	0.000	0.045	0.196	3.759	0.882	0.155	0.146	17	162	132(3;98.2) 173(4;1.5)
13	$FCl\cdots NH_2Cl$ (C_s)	1.685	2.379	6.90	0.046	−0.005	0.094	0.320	3.042	0.782	0.234	0.184	24	199	157(3;97.3) 254(4;2.4)
14	$FCl\cdots NH_2OH$ (C_s) *syn*	1.712	2.223	9.84	0.068	−0.016	0.179	0.451	2.472	0.696	0.379	0.242	35	254	208(3;98.6) 348(5;1.2)
	$FCl\cdots NH_2OH$ (C_s) *anti*	1.700	2.300	8.59	0.056	−0.010	0.138	0.430	2.697	0.731	0.285	0.206	28	220	182(3;97.8) 298(4;1.12) 87(1;1.0)
15	$FCl\cdots NH_2CH_3$ (C_s)	1.736	2.193	12.80	0.073	−0.019	0.217	0.551	2.239	0.658	0.497	0.281	43	290	239(3;92.5) 335(5;7.1)
16	$FCl\cdots OH_2$ (C_s)	1.660	2.566	4.75	0.024	0.002	0.032	0.178	3.967	0.909	0.170	0.154	17	162	145(3;99.9)
17	$FCl\cdots PF_3$ (C_{3v})	1.659	2.953	1.85	0.023	0.000	0.072	0.106	3.552	0.854	0.062	0.087	10	80	55(3;100)
18	$FCl\cdots PHF_2$ (C_s)	1.887	2.057	7.15	0.147	−0.087	0.561	0.242	1.209	0.465	0.909	0.396	85	306	228(3;95.0) 372(5;3.5) 432(6;1.4)
19	$FCl\cdots PH_2F$ (C_s)	1.883	2.104	7.88	0.133	−0.072	0.540	0.093	1.097	0.440	0.730	0.350	80	275	218(3;94.6) 383(4;5.3)
20	$FCl\cdots PH_3$ (C_{3v})	1.785	2.360	5.42	0.080	−0.026	0.361	0.361	0.654	0.329	0.121	0.127	39	112	106(1;100)
21	$FCl\cdots PH_2CN$ (C_s)	1.670	2.852	2.83	0.029	−0.002	0.073	0.147	2.857	0.755	0.069	0.092	12	85	73(2;100)
22	$FCl\cdots PH_2Cl$ (C_s)	1.840	2.195	5.44	0.110	−0.049	0.439	0.195	1.022	0.423	0.417	0.255	60	207	164(3;98.3) 325(4;1.7)
23	$FCl\cdots PH_2OH$ (C_s) *syn*	1.916	2.100	13.11	0.135	−0.076	0.609	0.286	1.095	0.440	0.905	0.395	90	306	283(4;99.1)
	$FCl\cdots PH_2OH$ (C_s) *anti*	1.904	2.102	10.12	0.134	−0.074	0.574	0.377	1.073	0.435	0.799	0.368	85	287	250(4;95.7) 352(5;4.3)
24	$FCl\cdots PH_2CH_3$ (C_s)	1.902	2.157	12.15	0.120	−0.060	0.567	0.383	1.039	0.427	0.701	0.342	80	269	244(4;95.5) 294(5;4.5)
25	$FCl\cdots SH_2$ (C_s)	1.673	2.863	4.31	0.027	−0.001	0.085	0.206	3.237	0.810	0.128	0.131	16	114	105(1;100)
NH_3 acceptor															
26	$HCCCl\cdots NH_3$ (C_{3v})	1.652	3.072	2.45	0.011	0.002	0.009	0.049	5.072	1.044	0.073	0.095	9	111	97(3;100)
27	$NCCl\cdots NH_3$ (C_{3v})	1.648	2.964	4.10	0.013	0.002	0.014	0.074	4.976	1.033	0.103	0.116	11	132	115(3;100)
28	$O_2NCl\cdots NH_3$ (C_s)	1.839	2.772	3.83	0.021	0.001	0.037	0.117	1.592	0.543	0.114	0.123	23	139	117(4;100)
29	$FH_2P\cdots NH_3$ (C_s)	1.644	2.663	6.10	0.025	−0.002	0.057	0.317	3.794	0.886	0.144	0.140	16	159	139(2;98.1) 148(3;1.9)
30	$FHS\cdots NH_3$ (C_s)	1.670	2.512	7.58	0.035	−0.003	0.081	0.410	3.309	0.820	0.194	0.166	20	184	163(3;99.9)
31	$FH\cdots NH_3$ (C_{3v})	0.953	1.695	12.11	0.053	−0.018	0.069	0.096	6.340	1.184	0.353	0.232	20	798	273(3;99.7)
Ionic systems															
32	$[F\cdots F\cdots F]^-$ ($D_{\infty h}$)	1.739	1.739	22.86	0.113	−0.027	0.584	0.367	1.376	0.500	1.376	0.500	100	496	398(3;28.5) 548(4;71.5)
33	$[Cl\cdots Cl\cdots Cl]^-$ ($D_{\infty h}$)	2.328	2.328	23.43	0.080	−0.022	0.546	0.465	0.701	0.342	0.701	0.342	100	261	260(3;90.3) 262(4;9.7)
34	$[Br\cdots Br\cdots Br]^-$ ($D_{\infty h}$)	2.594	2.594	26.21	0.062	−0.015	0.542	0.416	0.730	0.350	0.730	0.350	100	177	161(3;15.7) 184(4;84.3)
35	$[F\cdots Cl\cdots F]^-$ ($D_{\infty h}$)	1.875	1.875	45.01	0.121	−0.054	0.384	0.744	1.486	0.522	1.486	0.522	100	453	447(3;19.9) 455(4;80.1)
36	$[F\cdots H\cdots F]^-$ ($D_{\infty h}$)	1.140	1.140	43.21	0.178	−0.264	0.244	0.351	0.848	0.380	0.848	0.380	100	1226	1271(2;99.0)
37	$[F\cdots PH_2\cdots F]^-$ (C_2)	1.836	1.836	41.69	0.097	−0.068	0.277	0.812	1.257	0.475	1.257	0.475	100	308	413(3;20.0) 431(4;80.0)
38	$FCl\cdots Cl^-$ ($C_{\infty v}$)	1.883	2.316	28.98	0.081	−0.024	0.496	0.590	1.212	0.465	0.855	0.382	82	288	283(3;99.9)
39	$HCCCl\cdots Cl^-$ ($C_{\infty v}$)	1.657	3.025	8.11	0.018	0.001	0.046	0.138	4.599	0.988	0.166	0.152	15	127	114(3;100)
40	$NCCl\cdots Cl^-$ ($C_{\infty v}$)	1.659	2.883	16.59	0.024	0.000	0.072	0.190	4.126	0.929	0.247	0.190	20	155	140(3;100)
41	$O_2NCl\cdots Cl^-$ (C_{2v})	1.957	2.455	20.47	0.062	−0.013	0.378	0.474	0.732	0.350	0.487	0.278	79	217	214(3;98.5) 241(4;1.5)
42	$FH\cdots Cl^-$ ($C_{\infty v}$)	0.971	1.915	22.82	0.048	−0.017	0.115	0.186	5.355	1.076	0.415	0.254	24	848	255(1;99.5)
43	$FH_2P\cdots Cl^-$ (C_s)	1.725	2.649	18.62	0.039	−0.009	0.208	0.531	2.136	0.641	0.307	0.214	33	178	166(1;100)
44	$FHS\cdots Cl^-$ (C_s)	1.790	2.493	22.48	0.056	−0.014	0.305	0.581	1.466	0.518	0.443	0.264	51	212	204(1;99.4)

Donors

#	Complexes (*sym.*)	r	k^a	n	ω^a	V	#	Complexes (*sym.*)	r	k^a	n	ω^a	V
45	F_2	1.418	4.700	1.000	916	16.5	**50**	HCCCl	1.649	5.227	1.062	996	34.2
46	FCl	1.646	4.326	0.954	772	40.4	**51**	NCCl	1.644	5.209	1.060	995	36.8
47	Cl_2	2.019	3.025	0.780	542	25.4	**52**	H_2FP	1.577	5.791	1.125	914	36.6
48	Br_2	2.313	2.340	0.675	317	28.5	**53**	HFS	1.626	4.569	0.984	807	40.3
49	O_2NCl	1.864	1.403	0.506	488	21.9	**54**	FH	0.921	9.594	1.496	4125	68.3

[a] Computed at CCSD(T)/aug-cc-pVTZ. Bond distances r(XY) and r(XA) in Å, ΔE in kcal mol^{-1}, density at the XA critical point ρ_b in e Bohr^{-3}, energy density at XA critical point H_b in Hartree Bohr^{-3}, NBO intermonomer charge transfer (CT), local YXA bending force constant in mdyn Å rad^{-2}, local XY and XB stretching force constant in mdyn Å^{-1}, local stretching frequency ω^a in cm^{-1}, bond strength order n, 3c-4e% character calculated from n(XA)/n(XY), normal mode frequencies related to XA stretching ω_μ in cm^{-1} (normal mode number; %ω^a: % of local XA stretching character). In case of the X-donor monomers, the maximum electrostatic potential V computed on the 0.001 e Bohr^{-3} electron density surface for the σ-hole of X (V in kcal mol^{-1}) is also given.

Table 2 Minimum electrostatic potential V at lp(A)[a]

X-Acceptor	$V(\mathbf{r})$	X-Acceptor	$V(\mathbf{r})$
NR_3		PR_3	
NF_3	−2.2	PF_3	2.6
NH_3	−37.3	PH_3	−15.7
NHF_2	−16.1	PHF_2	−6.0
NH_2F	−27.9	PH_2F	−11.2
NH_2CH_3	−36.6	PH_2CH_3	−21.0
NH_2OH	−26.5	PH_2OH	−14.6
NH_2CN	−11.8	PH_2CN	−1.3
NH_2Cl	−27.1	PH_2Cl	−8.5
AR_2		Anions	
OH_2	−32.3	F^-	−168.6
SH_2	−16.5	Cl^-	−139.5
		Br^-	−131.6

[a] Minimum electrostatic potential V (kcal mol^{-1}) computed on the 0.001 e Bohr^{-3} electron density surface at lp(A). CCSD(T)/aug-cc-pVTZ.

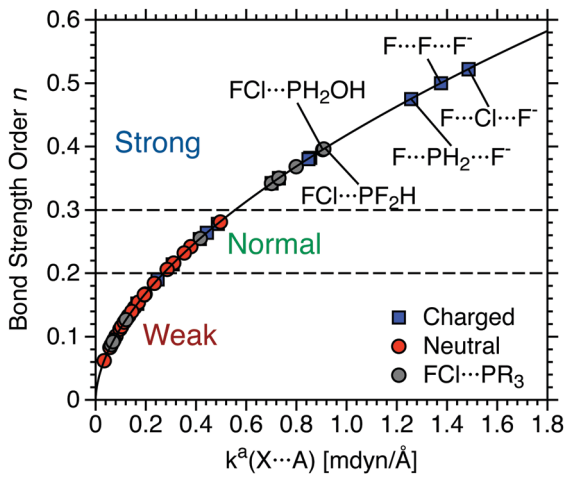

Fig. 2 Power relationship between the relative bond strength order (BSO) n and the local stretching force constants k^a of XB (halogen), HB (hydrogen), PB (pnicogen), and CB (chalcogen) bonding in complexes **1–44**. CCSD(T)/aug-cc-pVTZ calculations. See also Table 1 and Fig. 1.

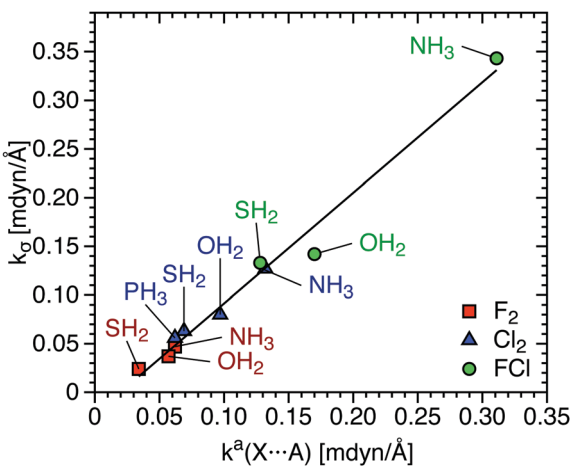

Fig. 3 Linear relationship between intermonomer stretching force constant k_σ measured by microwave spectroscopy[33] and local XB stretching force constants k^a calculated at CCSD(T)/aug-cc-pVTZ. R^2 = 0.983.

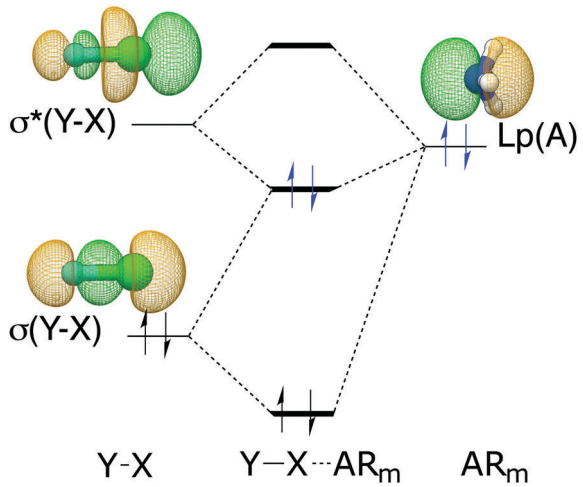

Fig. 4 Orbital interaction diagram showing the 2e-delocalization of an electron lone pair at the halogen acceptor (A) into the σ*(XY) orbital of the halogen donor XY.

lp(A) to the σ*(XY) orbital (Fig. 4) thus leading to 2e-delocalization and stabilization of lp(A). The magnitude of the 2e-delocalization is proportional to the orbital overlap and inversely proportional to the energy gap $\Delta\varepsilon(2e)$ between the energies of the lp(A) and the σ*(XY) orbital. As shown in Fig. 4, the 2e-stabilization effect is always accompanied by a 4e-destabilization effect involving lp(A) and the bonding σ(XY) orbital. The 2e-stabilization increases and the 4e-destabilization decreases when increasing the electronegativity of Y because this (i) lowers the energies of σ(XY) and σ*(XY) orbital (decrease of $\Delta\varepsilon(2e)$ and increase of $\Delta\varepsilon(4e)$) and (ii) increases the overlap between lp(A) and σ*(XY) (decreases the overlap between lp(A) and σ(XY) as the lower electronegativity of X leads to a smaller X coefficient. Because of orbital orthogonality, the X coefficient becomes larger in the σ*(XY) orbital). As a consequence of the charge transfer from lp(A) to σ*(XY) and the formation of the XB, the Y–X single bond is weakened (for exceptions, see Section 3).

The electrostatic part of the halogen bond depends on (i) the mutual polarization of the monomers and (ii) on the Coulomb attraction between a negatively charged heteroatom A and the σ-hole of X. The latter effect is relevant when Y has a larger electronegativity than X thus withdrawing σ charge from X and contracting the σ density at X and generating a σ-hole.[84,85] Dispersive contributions are smaller than the other contributions, but still non-negligible, especially for weak halogen bonds.[80]

We have determined the covalent character of the monomer interactions in complexes **1–44** (Fig. 1) utilizing the energy density H_b at the density critical point r_b between X and A (Fig. 5). There is a continuous transition from electrostatic (H_b close to zero) to covalent XB with negative H_b values indicating that electron density accumulation in the interaction region is stabilizing the complex. Utilizing the BSO values in Fig. 2, one can distinguish between weak predominantly electrostatic halogen bonds ($0.05 < n(XA) \leq 0.2$), normal halogen bonds ($0.2 < n(XA) \leq 0.3$), and strong, predominantly covalent halogen bonds ($0.3 < n(XA) < 0.6$). As shown in Fig. 2, XB

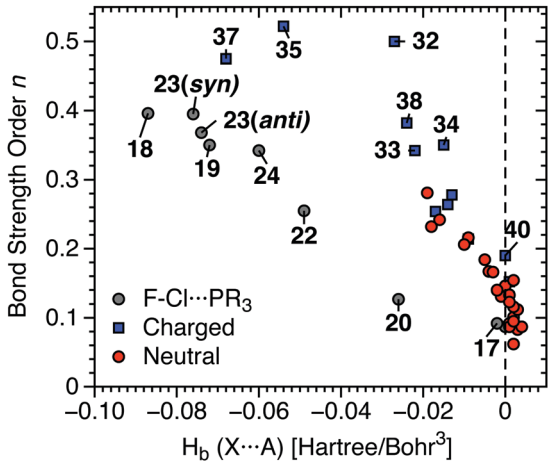

Fig. 5 Comparison of the bond strength order n with the energy density H_b at the density critical point of XB (halogen bonding), HB (hydrogen bonding), PB (pnicogen bonding), or CB (chalcogen bonding). H_b values close to zero indicate electrostatic and negative H_b values covalent bonding.[109,110] CCSD(T)/aug-cc-pVTZ. For the numbering of complexes, see Fig. 1.

varies over a BSO range larger than 0.5, which is significantly larger than found in the case of hydrogen bonding[95] and pnicogen bonding.[117,118]

Halogen bonding leading to a blue shift

There are cases of XB that lead to a shortening rather than lengthening of the XY bond.[75,76] For example, in complex **28** ($O_2NCl\cdots NH_3$) the NCl bond becomes shorter by 0.025 Å (reduction from 1.864 Å in the monomer to 1.839 Å in the complex; Table 1 and Table S3 in the ESI†). This leads to a blue shift in the NCl stretching frequency by 32 cm^{-1} (from 488 cm^{-1} in the monomer to 520 cm^{-1} in the XB-complex), which has to be compared with a blue shift of just 13 cm^{-1} in the normal mode frequencies that have strong N–Cl stretching character (monomer: 378 cm^{-1} (98.2% NCl stretching character); complex: 391 cm^{-1} (99.9%)). This underlines the advantages of carrying out the analysis in terms of local rather than normal modes. The cause of the strengthening of the NCl bond upon XB formation with NH_3 is a result of exchange repulsion between the monomers upon complex formation. The Lewis base NH_3 is a weak lp-density donor (charge transfer of just 0.037 e compared to 0.378 e of Cl^- in **41** ($O_2NCl\cdots Cl^-$); Table 1). Hence, exchange repulsion is a dominant force when the monomers are approaching. The electron density of the monomer O_2NCl is polarized, the NCl bond becomes more polar, and the NCl antibonding orbital is lowered in energy (see Fig. S5 in the ESI† for perspective drawings of the MOs). This leads to a stronger interaction with the ONO lp-orbitals in the sense of an anomeric interaction so that lp(O) density is transferred into the NCl bond (Jemmis has used the term "negative hyperconjugation" in this connection[75,76]). Normally, this would lead to bond weakening but due to the increased polarity of the NCl bond, the NCl antibonding character is decreased, and bond shortening rather than lengthening results during XB-complex formation with the Lewis base NH_3 as is nicely documented by the habitus of the XB-complex HOMO (see ESI†). Hence, exchange repulsion is the actual cause for the blue shift in the XY frequency.[119,120] The anion of Cl has a much more diffuse charge distribution that leads to less exchange repulsion, less polarization, and a larger charge transfer. Accordingly a lengthening of the N–Cl bond in **41** and a red shift of 136 cm^{-1} in the local NCl frequency is the consequence.

Halogen bonding in dihalogens and interhalogens

Fig. 6 gives the relative strength of the XB for a series of halogen donors Y in Y–X (F_2, Cl_2, FCl) and halogen acceptors AR_m (OH_2, NH_3, SH_2, PH_3). A stable halogen bonded $F_2\cdots PH_3$ complex could not be found at the CCSD(T) level because of the weakness of F···P interactions. All but complex **11** ($FCl\cdots NH_3$) of complexes **1–11** shown in Fig. 6 are weak and dominated by electrostatic interactions as is documented by the small BSO values and the positive (or weakly negative) H_b-values (Table 1).

Dihalogen F_2 leads to weak interactions with a Lewis base as the σ*(FF) orbital is strongly contracted. Therefore, it provides insufficient overlap with orbital lp(A). The corresponding XBs are relatively weak with n-values smaller than 0.1 (red squares in Fig. 6). Hence, it depends on the polarizing power of the acceptor AR_m and the electrostatic interactions between the monomers to establish a XB. The electrostatic potential values V at lp(A) are useful to explain trends in the calculated BSO(XB) values ($V(NH_3)$: −37.3 kcal mol^{-1} < $V(OH_2)$: −32.3 kcal mol^{-1} ≪ $V(SH_2)$: −16.5 < $V(PH_3)$: −15.7 kcal mol^{-1}, Table 2). Cl_2 can be better polarized than F_2 and has a more positive σ-hole ($V(F_2)$: 16.5; $V(Cl_2)$: 25.4 kcal mol^{-1}, Table 2), which leads to stronger but still dominantly electrostatic XBs (n < 0.15, blue triangles in Fig. 6).

Significantly stronger XBs are obtained in the case of an interhalogen such as FCl (green dots in Fig. 6). The electrostatic part of the interactions is enlarged due to the dipole moment of FCl (0.93 Debye, CCSD(T)), which increases the attraction

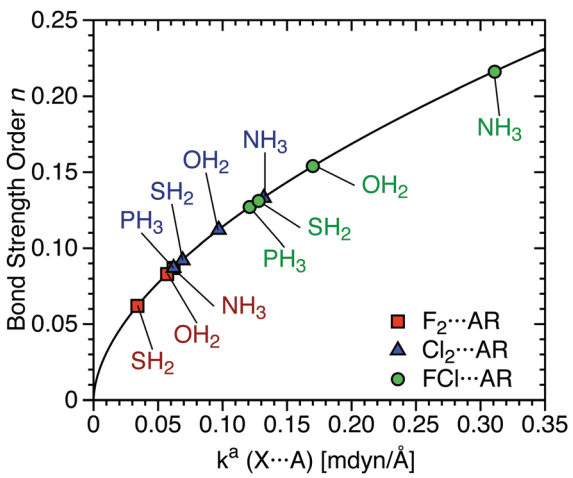

Fig. 6 Power relationship between the relative BSO n and the local XB stretching force constant k^a for XB complexes involving F_2, Cl_2 and FCl halogen donors and various acceptors. Calculated at CCSD(T)/aug-cc-pVTZ.

between the halogen X (partially positively charged) and the Lewis-base A (partially negatively charged). Additional covalent interactions lead to a larger variation in the BSO values ($0.13 < n < 0.22$). The antibonding FCl orbital is sufficiently low in energy to support a stronger charge transfer of 145 m_e (milli-electron) for **11** (Table 1). This becomes possible because of an enlarged Cl orbital coefficient in the σ*(FCl) orbital (Allred–Rochow electronegativities: $\chi(F) = 4.10 < \chi(Cl) = 2.83$[121]) and a larger overlap with the lp(A) orbital of the acceptor.

The charge transfer does not necessarily relate to the strength of a XB. For example, the BSO values of the complexes FCl···PH_3 (**20**) and FCl···NH_3 (**11**) are 0.127 and 0.216, respectively, whereas the corresponding charge transfer values are 361 and 145 m_e. The 2e-stabilizing interaction in **20** is largely offset by electrostatic repulsion between the positively charged Cl atom (131 m_e) and the positively charged P atom (389 m_e). Hence, the electrostatic part of the XB decides on the ordering of the BSO values in the case of the FCl complexes.

Influence of the acceptor

The nature of the XB strongly depends on the availability of the lp(A) electrons, the polarizing power, and the negative charge of the acceptor atom A. This is demonstrated for the 8 amine and 8 phosphine···ClF complexes shown in Fig. 7. The XB strength increases in the series $NF_3 < NHF_2 < NH_2CN < NH_2F < NH_2Cl < NH_3 < NH_2OH < NH_2CH_3$ whereas for the phosphine complexes the order is changed to $PF_3 \leq PH_2CN < PH_3 \ll PH_2Cl \ll PH_2CH_3 \leq PH_2F < PH_2OH \leq PHF_2$. The BSO values of the amine complexes vary from 0.10 to 0.28 and those of the phosphine complexes from 0.09 to 0.40 thus revealing that XB is more variable in the case of the phosphines.

The trend observed for the amines can be easily explained using the electrostatic description of XB, but considering in a few cases covalent contributions. Electronegative substituents such as F lower the negative charge at N and thereby the attraction between the positively charged Cl and atom A. Considering the number of electronegative substituents and their electronegativity (in the case of CN, the group electronegativity) one can explain the BSO (intrinsic strength) values of all amine complexes with n smaller or equal to that of NH_3. Unusually large are only the BSO value of F–Cl···NH_2OH (0.242) and that of F–Cl···NH_2CH_3 (0.281). In the latter case, the hyperconjugative effect of the methyl group increases the electron-donor ability of N thus leading to a larger charge transfer and a stronger admixture of covalent bonding.

In the case of the NH_2OH partner of FCl, one should expect an electrostatic effect and a BSO value larger than that of NH_2F (0.167) but smaller than that of NH_2Cl (0.184). The actual increase to the value of 0.242 can only be rationalized by analyzing the calculated equilibrium geometry. The OH group is placed in the mirror plane of the complex and *syn* with regard to the Cl atom. Although the H···Cl distance is 2.579 Å, a weak, electrostatic H-bond is established (stretching $k^a = 0.088$ mdyn Å^{-1}; BSO value: 0.111), which stabilizes the complex, leads to a relative short ClN distance of 2.223 Å (for NH_3: 2.320 Å), and the increase in the BSO value. If the OH group is forced into the *anti* position the BSO value is decreased to 0.206 which is slightly higher than one would expect from the electrostatic model.

XB in the phosphine complexes suffers from two electronic deficiencies both caused by the lp(P) orbital (lp(P) is too diffuse to make P a strongly polarizing atom; insufficient overlap with the σ*(FCl) orbital) so that charge cannot be transferred effectively and a more covalent interaction becomes possible. If the positive charge of P increases for example because of electronegative substituents, then the lp(P) is contracted, the polarizing power of P is increased, and a better overlap with the σ*(FCl) orbital leads to a better charge transfer. However, the latter effect will be limited because of increased P, Cl repulsion, a decrease of the orbital energy of lp(P), an increase of Δε(2e), and a reduction of the 2e-stabilization effect. In connection with the electrostatic effect, one has to consider that the partially positive charge of P is shielded to some extend by the lp(P) density in the direction of the Cl atom as is indicated by the negative electrostatic potential of the monomers ($V(PH_3)$: −15.7, $V(PFH_2)$: −11.2; $V(PHF_2)$: −6.0 kcal mol^{-1}; Table 2)

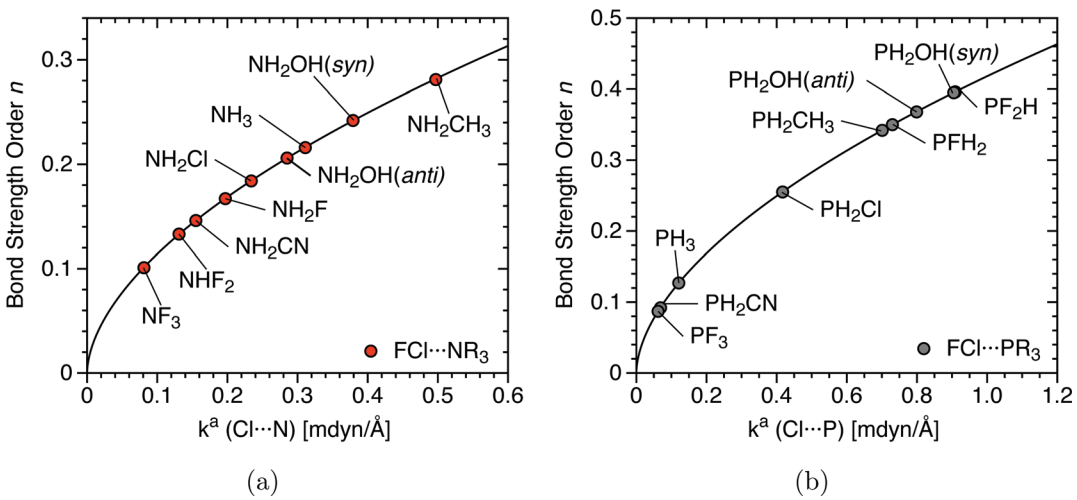

Fig. 7 Relationship between the relative BSO n and the local XB stretching force constant k^a, calculated at CCSD(T)/aug-cc-pVTZ. (a) Cl···N halogen bonding between FCl and eight amines. (b) Cl···P halogen bonding between FCl and eight phosphines.

with the only exception being ($V(PF_3)$: 2.55 kcal mol^{-1}; Table 2). There must be a compromise between the contraction of lp(P) (due to the electronegative substituents at P) and the enlargement of $\Delta\varepsilon$(2e) (reduction of 2e-stabilization).

For the XB-complex **17** (FCl$\cdots$PF$_3$), one might think of a σ-hole, σ-hole interaction and a mutual transfer of charge from the P to the Cl and from the Cl back to P in the sense of a mixed halogen–pnicogen bond. The calculated charge transfer of 0.072 *e* from Lewis base to X-donor suggests a dominance of XB. A pnicogen bond would lead to a lengthening of the PF bonds[117,118] whereas the calculated geometries indicate a reduction of the PF bonds from 1.580 (monomer) to 1.573 Å (complex) as it is typical of XB. Furthermore, one has to emphasize that the description in terms of σ-hole, lp interactions is in itself a model that excludes the effects of the kinetic energy and, therefore should not be pushed too far.

The charge transfer values of Table 1 and the difference density distributions shown in Fig. 8 provide an insight where the best compromise is achieved. For three F substituents as in PF$_3$, the increase in $\Delta\varepsilon$ is too large, 2e-stabilization and charge transfer are strongly reduced (72 m_e) compared to PH$_3$ (361 m_e) so that electrostatic interactions dominate XB. The difference density distributions confirm this in so far as for PF$_3$ just a small region of density increase between Cl and P (blue ball in Fig. 8) and a similar increase at the F atom is visible whereas for the PH$_3$ complex regions of charge increase and decrease alternate throughout the complex from the nonbonding region of the PH bonds to the lp(F) region, which is in line with charge transfer and charge polarization.

For the PHF$_2$, a clear increase in charge transfer (561 m_e, Table 1) and charge polarization is documented by the difference density distribution in Fig. 8. The charge transfer leads to a lengthening of the FCl bond from 1.785 (PH$_3$) to 1.887 Å (PHF$_2$), the ClP distance is reduced from 2.360 to 2.057 Å and the charge at the F(Cl) atom increases from 492 m_e (PH$_3$) to 632 m_e. The BSO value of the XB is 0.396 (PHF$_2$) whereas that of the FCl bond is reduced from 0.954 to 0.465 suggesting that the real structure is a superposition of the halogen-bonded complex and the ion pair F$^-\cdots$Cl–PHF$_2^+$. Such structures were first discussed by Alkorta and co-workers[49] and called chlorine shared bonds. It is more appropriate to consider them as a superposition of XB and 3c-4e-bonds (in short: 3c-4e XBs), which can be identified *via* (i) the large charge at the interhalogen F, (ii) the BSO values of F–Cl and Cl$\cdots$P which are similar or inverted, (iii) the difference density distributions with an increase in the XB and at the interhalogen F (Fig. 8), and (iv) delocalization of the lp(Cl) electrons into the σ*(PR) orbitals, especially into those of the PF bonds.

We quantify the amount of 3c-4e XB with the help of the calculated BSO(XY) and BSO(XB) values. If the latter is zero, there is no XB. If they are equal, there will be 100% 3c-4e XB. In general, the percentage of 3c-4e XB is given by the expression $100 \times n(AX)/n(XY)$. For amines these values are up to 40% (NH$_2$CH$_3$: 43%, Table 1). However, for the phosphines, they can increase to 90%: PH$_2$OH (90; 0.395) ≈ PHF$_2$ (85%; n(XB) = 0.396) > PH$_2$CH$_3$ (80) ≈ PH$_2$F (79) > PH$_2$Cl (60) > PH$_3$ (39).

3c-4e XBs are found for PH$_2$OH (n(ClP) = 0.395), which, as in the case of the corresponding amine complex, forms an electrostatic H-bond with Cl (r = 2.889 Å, k^a = 0.098 mdyn Å^{-1}, BSO value: 0.113; PH$_2$F: n(ClP) = 0.350; PH$_2$CH$_3$: n(ClP) = 0.342; PH$_2$Cl: n(ClP) = 0.255). Interesting is the PH$_2$CH$_3$ value as one could argue that in this case the hyperconjugative effect of a methyl group increases the Lewis-base character of the phosphine. Hyperconjugation also strengthens the electrostatic contribution. Even though the electronegativity of C (or the Me group) is larger than that of P (χ(C) = 2.50 > χ(P) = 2.06[121]), leading to an increase of the positive charge at P (801 compared to 389 m_e in **20** and 0.358 in PH$_2$CH$_3$ compared to 0.108 in PH$_3$)

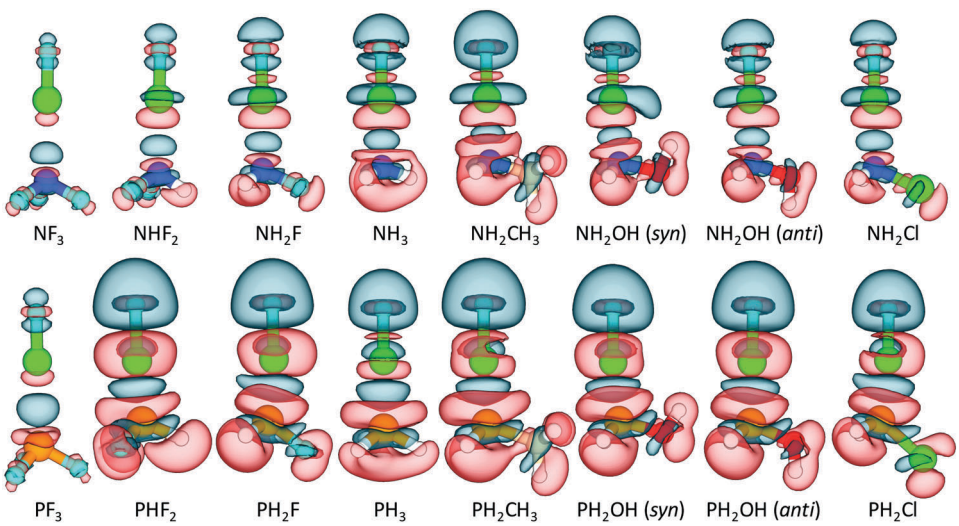

Fig. 8 CCSD(T)/aug-cc-pVTZ electron difference density distributions $\Delta\rho(\mathbf{r})$ given for FCl$\cdots$NR$_3$ and FCl$\cdots$PR$_3$ complexes. $\Delta\rho(\mathbf{r})$ is plotted for an electron density surface with a constant density value of 0.001 a.u. Blue regions indicate an increase in the electron density, red regions a density decrease relative to the superimposed density of the monomers.

there is a decrease of the electrostatic potential in the lone pair region ($V(PH_3)$: −15.7; $V(PH_2CH_3)$: −21.0 kcal mol^{-1}; Table 2).

Halogen bonding in anions

The ideal 3c-4e XB with 100% electron delocalization and therefore covalent nonclassical bonding (H_b < 0, Table 1) is realized for $[F\cdots F\cdots F]^-$ (**32**), which we have used as suitable reference with a BSO of 0.500. Anions $[Cl\cdots Cl\cdots Cl]^-$ (**33**) and $[Br\cdots Br\cdots Br]^-$ (**34**) have also 100% 3c-4e XB, but their BSO decreases to 0.342 and 0.350. The decrease is due to an increase of the σ orbital energies (because of decreasing electronegativity) and increased lp-repulsion between the pπ electrons of the halogen atoms. The latter becomes less destabilized with increasing X–X distance so that $[Br\cdots Br\cdots Br]^-$ has a somewhat larger BSO value (0.350) than $[Cl\cdots Cl\cdots Cl]^-$ (0.342). Since the negative charge is accumulated at the terminal atoms, the inclusion of a less electronegative atom such as Cl leads to an increase in the BSO to 0.522 (**35**), which is also reflected in its binding energy ΔE of 45.0 kcal mol^{-1} (Table 1). Such an increase is also found when H occupies the central position (**36**), but since H does not possess a 2pσ-orbital its BSO is just 0.380 (ΔE = 43.2 kcal mol^{-1}).

An unexpectedly strong 3c-4e bond is obtained if PH_2 is in the center of the anion (BSO: 0.475; ΔE = 41.7 kcal mol^{-1}) as in $[F\cdots PH_2\cdots F]^-$ (**37**). The complex has a butterfly form with long PF bonds (1.838 compared to the 1.577 Å of the PF bond in the monomer PFH_2). The molecule should be a suitable ligand for transition metal complexes or suitable for fluorination. Bonding in F_3^- and related halogen systems correspond to covalent (delocalized) XB, in $[F\cdots H\cdots F]^-$ to covalent (delocalized) H-bonding, and, accordingly, in $[F\cdots PH_2\cdots F]^-$ to covalent (delocalized) pnicogen bonding although the latter term is actually reserved for the non-covalent interactions of two pnicogens. One could also speak of hypervalent bonding as $PF_2H_2^-$ or PF_4^- are isoelectronic with the corresponding sulfur analogues difluorodihydrogen and tetrafluoro sulfurane. Compared to the axial SF bonds in these molecules (1.646 Å), the axial PF bonds are lengthened by 0.2 Å, which is due to the negative charge in the axial positions (see Fig. 1) entering the third and antibonding FPF orbital.

The local bending force constants k^a(YXA) provide an indirect indicator for the strength of the covalent 3c-4e bonds. A stiffer linear arrangement reflects a stronger covalent XB: $[Br\cdots Br\cdots Br]^-$ (k^a(YXA) mdyn Å rad^{-2}): (0.416; BSO: 0.350) ≈ $[Cl\cdots Cl\cdots Cl]^-$ (0.465; 0.342) < $[F\cdots F\cdots F]^-$ (0.367: 0.500) < $[F\cdots Cl\cdots F]^-$ (0.744; 0.522) < $[F\cdots PH_2\cdots F]^-$ (0.812; 0.475) < $[F\cdots H\cdots F]^-$ (0.351; 0.380). The comparison with the BSO values reveals that the bending force constants are useful, but do not provide a quantitative measure of the 3c-4e bond strength as the different size of the central atom (group) can lead to an increase of the bending force constant, which disguises the stiffness caused by 4e-delocalization in YXA.

3c-4e XB is partly lost if the symmetry of the complex is reduced by substituting one of the terminal halogens by another group. Table 1 reveals that in the series $O_2NCl\cdots Cl^-$ (79% of 3c-4e bonding; n(XA) = 0.278) > $FCl\cdots Cl^-$ (82%; 0.382) > $FSH\cdots Cl^-$ (51%; 0.264) > $FH_2P\cdots Cl^-$ (33%; 0.214) > $FH\cdots Cl^-$ (24%; 0.254) > $NCCl\cdots Cl^-$ (20%; 0.190) > $HCCCl\cdots Cl^-$ (15%; 0.152) the 3c-4e bonding is successively lost, which is (partly) in line with a weakening of the XA covalent interactions as reflected by BSO, H_b, and charge transfer values. Clearly, the higher the energy of the acceptor orbital σ*(XY) is (the lower the electronegativity of the donor Y), the weaker is the actual XB and the lower is the degree of 3c-4e delocalization. It is interesting to note that chalcogen bonding as in $F(H)S\cdots Cl^-$ (**44**) is stronger than pnicogen bonding in $FH_2P\cdots Cl^-$ (**43**) or H-bonding in $FH\cdots Cl^-$ (**42**). In Fig. 9, examples of stronger and weaker XBs are shown.

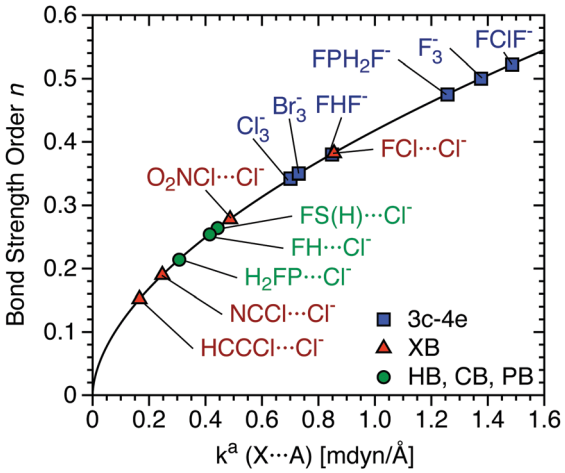

Fig. 9 Relationship between the relative BSO n and the local XB stretching force constant k^a for ionic complexes. See text. CCSD(T)/aug-cc-pVTZ calculations.

Non-covalent interactions in neutral systems: comparison of halogen bonding with chalcogen, pnicogen, and H-bonding

Considering ammonia as a prototypical neutral acceptor, two series of complexes were compared: (i) XBs for different X-donors (FCl, Cl_2, O_2NCl, NCCl, HCCCl) where a Cl atom

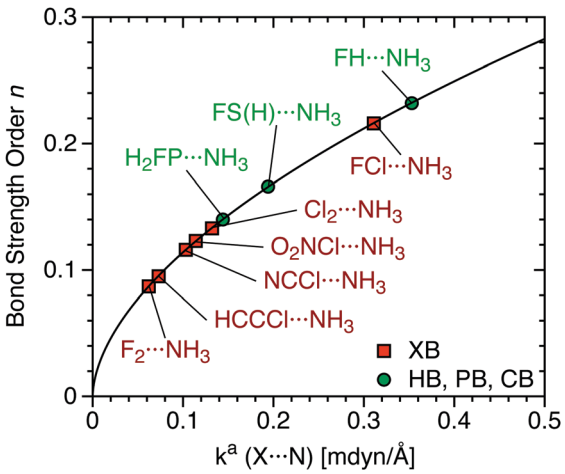

Fig. 10 Relationship between the relative BSO n and the local XB stretching force constant k^a for complexes between NH_3 and a halogen (YX), pnicogen (H_2FP), chalcogen (F(H)S) or hydrogen bonding partner (FH). CCSD(T)/aug-cc-pVTZ calculations.

interacts with the N atom of NH_3. (ii) The XB in $FCl\cdots NH_3$ was compared with other types of non-covalent interactions such as H-bonding in $FH\cdots NH_3$, pnicogen-bonding in $H_2FP\cdots NH_3$ and chalcogen bonding in $F(H)S\cdots NH_3$. In these complexes, electrostatic interactions can be complemented by a charge transfer from lp(N) to the σ* orbital of the halogen, hydrogen, pnicogen, or chalcogen donor.

According to Fig. 10 the polarity of the Y–X bonds and the polarizability of X decide on the magnitude of the electrostatic interactions, which should increase in the series Y–X: F–F (0.087) < HCCCl (0.095) < NCCl (0.116) < O_2NCl (0.123) < Cl_2 (0.133) < H_2FP (0.140) < F(H)S (0.166) < FCl (0.216) < FH (0.232). There are also minor covalent interactions as is reflected by the charge transfer values especially in the case of $Cl_2\cdots NH_3$ (55 m_e) compared to $NCCl\cdots NH_3$ (14 m_e), leading to a stronger XB even though NCCl has a more positive electrostatic potential (V(NCCl): 36.8; $V(Cl_2)$: 25.4 kcal mol^{-1}). Larger charge transfer values are found for the chalcogen bond of $F(H)S\cdots NH_3$ (81 m_e), the pnicogen bond of $H_2FP\cdots NH_3$ (57 m_e), the H-bond of $FH\cdots NH_3$ (69 m_e), and the XB in $FCl\cdots NH_3$ (145 m_e). In all these cases, a lengthening of the charge acceptor bond is observed (from 1.626 to 1.670; 1.577 to 1.644, 0.921 to 0.953, and 1.646 to 1.703 Å, Table 1).

Clearly, the XB is stronger than the chalcogen or pnicogen bond if one compares the three non-covalent interactions $FCl\cdots NH_3$, $F(H)S\cdots NH_3$, and $H_2FP\cdots NH_3$. This is the result of three electronic factors: (i) because Cl has a smaller covalent radius than S or P, FCl can establish a stronger interaction with larger orbital overlap. (ii) Due to the high electronegativity of both F and Cl, the energy of the σ*(XY) orbital is lower leading to a smaller Δε(2e) and a stronger 2e-destabilizing interaction. (iii) FCl forms a head-on interaction with NH_3 thus maximizing charge transfer (covalent interactions because of 2e-delocalization and stabilization) and electrostatic interactions (*via* a σ-hole).

If the non-covalent interactions between the monomers have an increasing charge transfer contribution, orbital overlap S is maximized, and the geometry leading to a maximal S becomes less flexible. Hence, the rigidity of the YXA unit measured by the local bending force constant k^a(YXA) increases for an increased covalent contribution to the $YX\cdots AR$ interactions. The values of k^a(YXA) listed in Table 1 reflect this: 0.434 ($FCl\cdots NH_3$) > 0.410 ($F(H)S\cdots NH_3$) > 0.317 ($H_2FP\cdots NH_3$) > 0.096 mdyn Å rad^{-2} ($FH\cdots NH_3$). Important in this connection is that one compares non-covalent interactions of the same type. Clearly, the H-bonding interactions as a first row-second row interaction should not be compared with a third row-second row interaction. Exchange repulsion between lp(X), lp(A), and AR bonding electrons is no longer present so that the H-bond in $FH\cdots NH_3$ (n = 0.232, see above) becomes stronger than the other non-covalent interactions.

Comparison of BSO values with other quantities

We have investigated whether the intrinsic strength of the XB is related to the distance r(XA), the binding energy, or the energy density at the critical point. The latter quantities are commonly discussed in the literature to assess the strength of the XB.[10] However, there is no relationship for example between the XB strength and the binding energy ΔE as the latter is a cumulative quantity that accounts not only for the intrinsic strength of the XB, but also for the energy required for the reorganization of the electronic structure of the monomer upon the formation of the complex and for contributions due to secondary inter-monomer interactions. Accordingly, a strong scattering of the data points is obtained when correlating BSO and ΔE (rXA,H_b) values for a larger set of complexes as we have done in the ESI† (not always done in the literature[49,72]) thus indicating that none of the latter quantities reflects the strength of the XB and therefore cannot be used for a quantitative ordering of XBs according to their strength. Even qualitatively, these quantities are limited to the description of small groups of XB systems dominated by similar electronic effects. As the BSO values derived from the local $X\cdots A$ stretching force constants provide a measure of the intrinsic strength of the bond, it is possible to discuss the strength of XB in a comparative, quantitative manner.

4 Conclusions and outlook

In this work, we present for the first time a quantitative description of the intrinsic strength of XB based on accurate CCSD(T)/aug-cc-pVTZ calculations of the local stretching force constant and an accurate analysis of binding energies, geometries, NBO charges, charge transfer values, dipole moments, electrostatic potentials, electron and energy density distributions, difference density distributions, vibrational frequencies, local bending force constants, and relative BSO values n all calculated at the coupled cluster level. In this way, a clear picture of the bonding mechanism emerges. XB has been compared with hydrogen, chalcogen, and pnicogen bonding where the latter term has been extended to include the interaction between a pnicogen atom and a hetero atom other than a pnicogen.

(1) XB can emerge from weak electrostatic interactions (binding energies ΔE < 10 kcal mol^{-1}) or from fully covalent 3c-4e interactions (ΔE up to 45 kcal mol^{-1}). The majority of XBs have both electrostatic and covalent interactions and therefore span a large range of binding energies and BSO values. Based on the local XB stretching force constant, we suggest to distinguish between weak electrostatic XBs (0.05 < n(XA) ≤ 0.2), normal XBs (0.2 < n(XA) ≤ 0.3), and strong, predominantly covalent XBs (0.3 < n(XA) < 0.6, Fig. 2).

(2) The mechanism of XB as it was repeatedly described in the literature[10] has been confirmed in this work. The covalent part can be rationalized by the orbital diagram of Fig. 4 and is characterized by charge transfer values or the difference density distribution of Fig. 8. We show that the 4e-destabilizing factor must not be overlooked when analyzing XB.

(3) The electrostatic part of XB increases with (i) the polarizing power of the hetero atom A, (ii) the polarity of the XY bond, and (iii) the polarizability of the halogen atom X. This implies that halogens X_2 with higher atomic number form stronger XBs and that in turn interhalogens XY form stronger XBs than dihalogens X_2 where the strongest bonds for a series of

interhalogens are found for Y = F. Deviations from these trends normally indicate covalent contributions to XB as in the case $FCl\cdots NH_3$.

(4) Electronegative substituents R attached to A can have opposing effects on the strength of the XB. The latter is reduced in the case of an amine because the negative charge at N is lowered and X···N attraction is reduced (*e.g.*, in $FCl\cdots NH_mR_{3-m}$ (m = 1, 2, 3) complexes). This effect is even stronger for phosphines. But in this case it is annihilated by a stabilizing covalent effect, which is based on the contraction of the lp(P) orbital and an improved overlap with the σ*(XY) orbital. Comparison of the calculated BSO and charge transfer values reveals that an optimal covalent contribution is obtained for the complex $FCl\cdots PHF_2$.

(5) XB can be strengthened by H bonding as we have demonstrated for the complexes $FCl\cdots NH_2OH$ and $FCl\cdots PH_2OH$. A *syn*-arrangement of the XB and the OH group leads to an electrostatic lp(Cl)···H–O bond with BSO values of 0.111 and 0.113 which increases the strength of the XB significantly. In the *anti* position, the effect of the OH group is destabilizing for amines and moderately stabilizing for phosphines.

(6) XB in substituted phosphines (R being more electronegative than P) leads to partial 3c-4e character, which can be quantified with the help of the BSO values: PH_2OH (90% of 3c-4e bonding; BSO = 0.395) ≈ PHF_2 (85%; n(AX) = 0.396) > PH_2CH_3 (80%) ≈ PH_2F (79%) > PH_2Cl (60%) > PH_3 (39%).

(7) 3c-4e bonding implies covalent character, which is completely fulfilled for anions of the type Y···X···Y (X,Y: halogen): $[Cl\cdots Cl\cdots Cl]^-$ (BSO: 0.342) < $[Br\cdots Br\cdots Br]^-$ (0.350) < $[F\cdots F\cdots F]^-$ (0.500) < $[F\cdots Cl\cdots F]^-$ (0.522). This trend of increasing bond strengths is due to increasing covalent interactions and better charge distributions.

(8) Halogen bonding is stronger than pnicogen, chalcogen, or H bonding in comparable complexes. One obtains for the following anions: $[F\cdots Cl\cdots F]^-$ (0.522) > $[F\cdots PH_2\cdots F]^-$ (0.475) > $[F\cdots H\cdots F]^-$ (0.380); neutral complexes: $FCl\cdots NH_3$ (0.216) > $F(H)S\cdots NH_3$ (0.166) > $H_2FP\cdots NH_3$ (0.140). In the latter case H-bonding is stronger because of the lack of destabilizing exchange repulsion: $FH\cdots NH_3$ (0.232). The strength of the XB is due to the smaller covalent radius of a halogen (compared to pnicogen, chalcogen), the larger overlap, the lower σ-orbital energies, and the larger 2e-stabilization effect.

(9) The intrinsic XB strength as measured by the BSO values is not reflected by the binding energies ΔE or the distance r(AX) because these parameters contain other effects, which are not related to the XB strength. The Badger rule (relationship between k^a(AX) and r(AX))[106,122] is only qualitatively fulfilled. The same holds for the charge transfer values, the density and energy distribution, ρ_b and H_b values, or the bending force constants k^a(YXA). These are useful quantities when discussing special electronic effects, but in general they do not reflect the intrinsic bond strength.

(10) All systems investigated were also calculated with several XC functionals. In general, DFT can give a qualitative correct description of XB, with few exceptions found for the F_2 complexes, and in those cases where strongly electronegative substituents and/or 3c-4e bonding are involved.

Future work has to show how XB changes with increasing atomic numbers for X and A to see how relativistic effects influence XB. One other topic, which deserves more attention is the description of XB *via* the σ-hole mechanism. Any form of bonding implies changes in both the potential and the kinetic energy as was demonstrated by Ruedenberg when investigating the H_2^+ and H_2 bond.[123,124] If one exclusively focuses on the potential energy, then the kinetic energy as an important component of bonding is neglected and conclusions just drawn on the existence of a $V(\mathbf{r})$-based ''σ-hole'' become questionable. Clearly, this aspect deserves additional investigation.

Acknowledgements

This work was financially supported by the National Science Foundation grants CHE 1152357 and CHE 1464906. We thank SMU for providing computational resources. The authors acknowledge financial support by CAPES (Brazil; fellowship grant BEX 9534-13-0).

References

1 M. C. Ford and P. S. Ho, Computational Tools To Model Halogen Bonds in Medicinal Chemistry, *J. Med. Chem.*, 2016, **59**, 1655–1670.
2 P. Ho, in *Halogen*, ed. I. Bonding, P. Metrangolo and G. Resnati, Topics in Current Chemistry, Springer International Publishing, 2015, vol. 358, pp. 241–276.
3 R. Wilcken, M. O. Zimmermann, A. Lange, A. C. Joerger and F. M. Boeckler, Principles and Applications of Halogen Bonding in Medicinal Chemistry and Chemical Biology, *J. Med. Chem.*, 2013, **56**, 1363–1388.
4 A. Abate, M. Saliba, D. J. Hollman, S. D. Stranks, K. Wojciechowski, R. Avolio, G. Grancini, A. Petrozza and H. J. Snaith, Supramolecular Halogen Bond Passivation of Organic-Inorganic Halide Perovskite Solar Cells, *Nano Lett.*, 2014, **14**, 3247–3254.
5 L. C. Gilday, S. W. Robinson, T. A. Barendt, M. J. Langton, B. R. Mullaney and P. D. Beer, Halogen Bonding in Supramolecular Chemistry, *Chem. Rev.*, 2015, **115**, 7118–7195.
6 C. B. Aakeroy, C. L. Spartz, S. Dembowski, S. Dwyre and J. Desper, A systematic structural study of halogen bonding *versus* hydrogen bonding within competitive supramolecular systems, *IUCrJ*, 2015, **2**, 498–510.
7 C. B. Aakeroy, T. K. Wijethunga, J. Desper and M. Dakovic, Crystal Engineering with Iodoethynylnitrobenzenes: A Group of Highly Effective Halogen-Bond Donors, *Cryst. Growth Des.*, 2015, **15**, 3853–3861.
8 O. Dumele, N. Trapp and F. Diederich, Halogen Bonding Molecular Capsules, *Angew. Chem., Int. Ed.*, 2015, **54**, 12339–12344.
9 G. Berger, J. Soubhye and F. Meyer, Halogen bonding in polymer science: from crystal engineering to functional supramolecular polymers and materials, *Polym. Chem.*, 2015, **6**, 3559–3580.

10 G. Cavallo, P. Metrangolo, R. Milani, T. Pilati, A. Priimagi, G. Resnati and G. Terraneo, The Halogen Bond, *Chem. Rev.*, 2016, **116**, 2478–2601.
11 O. Dumele, D. Wu, N. Trapp, N. Goroff and F. Diederich, Halogen Bonding of (Iodoethynyl)benzene Derivatives in Solution, *Org. Lett.*, 2014, **16**, 4722–4725.
12 N. Nagels, Y. Geboes, B. Pinter, F. DeProft and W. A. Herrebout, Tuning the Halogen/Hydrogen Bond Competition: A Spectroscopic and Conceptual DFT Study of Some Model Complexes Involving CHF2I, *Chem. – Eur. J.*, 2014, **20**, 8433–8443.
13 A. Bauzá, T. J. Mooibroek and A. Frontera, The Bright Future of Unconventional σ/π-Hole Interactions, *ChemPhysChem*, 2015, **16**, 2496–2517.
14 M. Saito, N. Tsuji, Y. Kobayashi and Y. Takemoto, Direct Dehydroxylative Coupling Reaction of Alcohols with Organosilanes through Si–X Bond Activation by Halogen Bonding, *Org. Lett.*, 2015, **17**, 3000–3003.
15 C. B. Aakeroy, T. K. Wijethunga, J. Desper and C. Moore, Halogen-Bond Preferences in Co-crystal Synthesis, *J. Chem. Crystallogr.*, 2015, **45**, 267–276.
16 S. Schindler and S. M. Huber, in *Halogen Bonding II*, ed. P. Metrangolo and G. Resnati, Topics in Current Chemistry, Springer International Publishing, 2015, vol. 359, pp. 167–203.
17 F. Kniep, S. H. Jungbauer, Q. Zhang, S. M. Walter, S. Schindler, I. Schnapperelle, E. Herdtweck and S. M. Huber, Organocatalysis by Neutral Multidentate Halogen-Bond Donors, *Angew. Chem., Int. Ed.*, 2013, **52**, 7028–7032.
18 W. T. Pennington, T. W. Hanks and H. D. Arman, in *Halogen Bonding*, ed. P. Metrangolo and G. Resnati, Structure and Bonding, Springer Berlin Heidelberg, 2008, vol. 126, pp. 65–104.
19 T. M. Beale, M. G. Chudzinski, M. G. Sarwar and M. S. Taylor, Halogen bonding in solution: thermodynamics and applications, *Chem. Soc. Rev.*, 2013, **42**, 1667–1680.
20 L. P. Wolters, P. Schyman, M. J. Pavan, W. L. Jorgensen, F. M. Bickelhaupt and S. Kozuch, The many faces of halogen bonding: a review of theoretical models and methods, *Wiley Interdiscip. Rev.: Comput. Mol. Sci.*, 2014, **4**, 523–540.
21 A. V. Jentzsch and S. Matile, in *Halogen Bonding I*, ed. P. Metrangolo and G. Resnati, Topics in Current Chemistry, Springer International Publishing, 2015, vol. 358, pp. 205–239.
22 M. H. Kolar and P. Hobza, Computer Modeling of Halogen Bonds and Other σ-Hole Interactions, *Chem. Rev.*, 2016, **116**, 5155–5187.
23 P. Metrangolo, F. Meyer, T. Pilati, G. Resnati and G. Terraneo, Halogen Bonding in Supramolecular Chemistry, *Angew. Chem., Int. Ed.*, 2008, **47**, 6114–6127.
24 E. Parisini, P. Metrangolo, T. Pilati, G. Resnati and G. Terraneo, Halogen Bonding in Halocarbon-Protein Complexes: A Structural Survey, *Chem. Soc. Rev.*, 2011, **40**, 2267–2278.
25 G. Terraneo, G. Resnati and P. Metrangolo, *Iodine Chemistry and Applications*, John Wiley and Sons, Inc., 2014, pp. 159–194.
26 A. C. Legon, Prereactive Complexes of Dihalogens XY with Lewis Bases B in the Gas Phase: A Systematic Case for the Halogen Analogue B···XY of the Hydrogen Bond B···HX, *Angew. Chem., Int. Ed.*, 1999, **38**, 2686–2714.
27 M. C. A. Aragoni, M. Devillanova, F. A. Garau, A. Isaia, F. Lippolis and V. M. Annalisa, The nature of the chemical bond in linear three-body systems: from I_3^- to mixed chalcogen/halogen and trichalcogen moieties, *Bioinorg. Chem. Appl.*, 2007, **2007**, 1–46.
28 B. Braida and P. C. Hiberty, Application of the valence bond mixing configuration diagrams to hypervalency in trihalide anions: a challenge to the-rundle-pimentel model, *J. Phys. Chem. A*, 2008, **112**, 13045–13052.
29 J. E. Del Bene, I. Alkorta and J. Elguero, Do Traditional, Chlorine-shared, and Ion-pair Halogen Bonds Exist? An ab Initio Investigation of FCl:CNX Complexes, *J. Phys. Chem. A*, 2010, **114**, 12958–12962.
30 J. E. Del Bene, I. Alkorta and J. Elguero, Do nitrogen bases form chlorine-shared and ion-pair halogen bonds?, *Chem. Phys. Lett.*, 2011, **508**, 6–9.
31 O. Donoso-tauda, P. Jaque, I. Alkorta, J. Elguero and I. Alkorta, Traditional and ion-pair halogen-bonded complexes between chlorine and bromine derivatives and a nitrogen-heterocyclic carbene, *J. Phys. Chem. A*, 2014, **118**, 9552–9560.
32 J. Rezac and P. Hobza, Benchmark Calculations of Interaction Energies in Noncovalent Complexes and Their Applications, *Chem. Rev.*, 2016, **116**, 5038–5071.
33 A. C. Legon, A reduced radial potential energy function for the halogen bond and the hydrogen bond in complexes B···XY and B···HX, where X and Y are halogen atoms, *Phys. Chem. Chem. Phys.*, 2014, **16**, 12415–12421.
34 A. O. de-la Roza, E. R. Johnson and G. A. DiLabio, Halogen Bonding from Dispersion-Corrected Density-Functional Theory: The Role of Delocalization Error, *J. Chem. Theory Comput.*, 2014, **10**, 5436–5447.
35 J. G. Hill and X. Hu, Theoretical Insights into the Nature of Halogen Bonding in Prereactive Complexes, *Chem. – Eur. J.*, 2013, **19**, 3620–3628.
36 A. Karpfen, *Halogen Bonding*, 2008, vol. 126, pp. 1–15.
37 B. Braida and P. C. Hiberty, Application of the Valence Bond Mixing Configuration Diagrams to Hypervalency in Trihalide Anions: A Challenge to the Rundle-Pimentel Model, *J. Phys. Chem. A*, 2008, **112**, 13045–13052.
38 S. Kozuch and J. M. L. Martin, Halogen Bonds: Benchmarks and Theoretical Analysis, *J. Chem. Theory Comput.*, 2013, **9**, 1918–1931.
39 J. Grant Hill, The halogen bond in thiirane···ClF: an example of a Mulliken inner complex, *Phys. Chem. Chem. Phys.*, 2014, **16**, 19137–19140.
40 J. Grant Hill and A. C. Legon, On the directionality and non-linearity of halogen and hydrogen bonds, *Phys. Chem. Chem. Phys.*, 2015, **17**, 858–867.
41 A. Forni, S. Pieraccini, S. Rendine and M. Sironi, Halogen bonds with benzene: an assessment of DFT functionals, *J. Comput. Chem.*, 2014, **35**, 386–394.
42 L. P. Wolters and F. M. Bickelhaupt, Halogen Bonding *versus* Hydrogen Bonding: A Molecular Orbital Perspective, *ChemistryOpen*, 2012, **1**, 96–105.

43 B. Pinter, N. Nagels, W. A. Herrebout and F. DeProft, Halogen Bonding from a Hard and Soft Acids and Bases Perspective: Investigation by Using Density Functional Theory Reactivity Indices, *Chem. – Eur. J.*, 2013, **19**, 519–530.
44 V. Tognetti and L. Joubert, Electron density Laplacian and halogen bonds, *Theor. Chem. Acc.*, 2015, **134**, 1–10.
45 C. Wang, D. Danovich, Y. Mo and S. Shaik, On The Nature of the Halogen Bond, *J. Chem. Theory Comput.*, 2014, **10**, 3726–3737.
46 J. George, V. L. Deringer and R. Dronskowski, Cooperativity of Halogen, Chalcogen, and Pnictogen Bonds in Infinite Molecular Chains by Electronic Structure Theory, *J. Phys. Chem. A*, 2014, **118**, 3193–3200.
47 A. J. Parker, J. Stewart, K. J. Donald and C. A. Parish, Halogen Bonding in DNA Base Pairs, *J. Am. Chem. Soc.*, 2012, **134**, 5165–5172.
48 M. Palusiak, On the nature of halogen bond – The Kohn–Sham molecular orbital approach, *THEOCHEM*, 2010, **945**, 89–92.
49 J. E. D. Bene, I. Alkorta and J. Elguero, Influence of Substituent Effects on the Formation of P···Cl Pnicogen Bonds or Halogen Bonds, *J. Phys. Chem. A*, 2014, **118**, 2360–2366.
50 M. Tawfik and K. J. Donald, Halogen Bonding: Unifying Perspectives on Organic and Inorganic Cases, *J. Phys. Chem. A*, 2014, **118**, 10090–10100.
51 E. V. Bartashevich and V. G. Tsirelson, Interplay between non-covalent interactions in complexes and crystals with halogen bonds, *Russ. Chem. Rev.*, 2014, **83**, 1181.
52 D. J. R. Duarte, N. M. Peruchena and I. Alkorta, Double Hole-Lump Interaction between Halogen Atoms, *J. Phys. Chem. A*, 2015, **119**, 3746–3752.
53 H. J. Jahromi, K. Eskandari and A. Alizadeh, Comparison of halogen bonds in M–X···N contacts (M = C, Si, Ge and X = Cl, Br), *J. Mol. Model.*, 2015, **21**, 1–9.
54 R. Lo and B. Ganguly, Revealing halogen bonding interactions with anomeric systems: an *ab initio* quantum chemical studies, *J. Mol. Graphics Modell.*, 2015, **55**, 123–133.
55 V. Sladek, P. Skorna, P. Poliak and V. Lukes, The *ab initio* study of halogen and hydrogen σN-bonded *para*-substituted pyridine···(X2/XY/HX) complexes, *Chem. Phys. Lett.*, 2015, **619**, 7–13.
56 I. Alkorta, J. Elguero, O. Mo, M. Yanez and J. E. Del Bene, Using beryllium bonds to change halogen bonds from traditional to chlorine-shared to ion-pair bonds, *Phys. Chem. Chem. Phys.*, 2015, **17**, 2259–2267.
57 B. Nepal and S. Scheiner, Long-range behavior of non-covalent bonds. Neutral and charged H-bonds, pnicogen, chalcogen, and halogen bonds, *Chem. Phys.*, 2015, **456**, 34–40.
58 S. M. Huber, E. Jimenez-Izal, J. M. Ugalde and I. Infante, Unexpected trends in halogen-bond based noncovalent adducts, *Chem. Commun.*, 2012, **48**, 7708–7710.
59 I. Alkorta, F. Blanco, M. Solimannejad and J. Elguero, Competition of Hydrogen Bonds and Halogen Bonds in Complexes of Hypohalous Acids with Nitrogenated Bases, *J. Phys. Chem. A*, 2008, **112**, 10856–10863.
60 U. Adhikari and S. Scheiner, Substituent Effects on Cl···N, S···N, and P···N Noncovalent Bonds, *J. Phys. Chem. A*, 2012, **116**, 3487–3497.
61 K. E. Riley, J. S. Murray, J. Fanfrlík, J. Rezác, R. J. Solá, M. C. Concha, F. M. Ramos and P. Politzer, Halogen bond tunability II: the varying roles of electrostatic and dispersion contributions to attraction in halogen bonds, *J. Mol. Model.*, 2013, **19**, 4651–4659.
62 A. J. Stone, Are Halogen Bonded Structures Electrostatically Driven?, *J. Am. Chem. Soc.*, 2013, **135**, 7005–7009.
63 R. Sedlak, M. H. Kolár and P. Hobza, Polar Flattening and the Strength of Halogen Bonding, *J. Chem. Theory Comput.*, 2015, **11**, 4727–4732.
64 W. Zierkiewicz, D. C. Bienko, D. Michalska and T. Zeegers-Huyskens, Theoretical investigation of the halogen bonded complexes between carbonyl bases and molecular chlorine, *J. Comput. Chem.*, 2015, **36**, 821–832.
65 K. Dyduch, M. P. Mitoraj and A. Michalak, ETS-NOCV description of σ-hole bonding, *J. Mol. Model.*, 2013, **19**, 2747–2758.
66 M. P. Mitoraj and A. Michalak, Theoretical description of halogen bonding – an insight based on the natural orbitals for chemical valence combined with the extended-transition-state method (ETS-NOCV), *J. Mol. Model.*, 2013, **19**, 4681–4688.
67 E. V. Bartashevich and V. G. Tsirelson, Atomic dipole polarization in charge-transfer complexes with halogen bonding, *Phys. Chem. Chem. Phys.*, 2013, **15**, 2530–2538.
68 D. Duarte, G. Sosa and N. Peruchena, Nature of halogen bonding. A study based on the topological analysis of the Laplacian of the electron charge density and an energy decomposition analysis, *J. Mol. Model.*, 2013, **19**, 2035–2041.
69 E. L. Angelina, D. R. Duarte and N. M. Peruchena, Is the decrease of the total electron energy density a covalence indicator in hydrogen and halogen bonds?, *J. Mol. Model.*, 2013, **19**, 2097–2106.
70 S. J. Grabowski, Non-covalent interactions – QTAIM and NBO analysis, *J. Mol. Model.*, 2013, **19**, 4713–4721.
71 D. Duarte, E. L. Angelina and N. Peruchena, Physical meaning of the QTAIM topological parameters in hydrogen bonding, *J. Mol. Model.*, 2014, **20**, 1–10.
72 A. Shahi and E. Arunan, Hydrogen bonding, halogen bonding and lithium bonding: an atoms in molecules and natural bond orbital perspective towards conservation of total bond order, inter- and intra-molecular bonding, *Phys. Chem. Chem. Phys.*, 2014, **16**, 22935–22952.
73 D. Kaur, R. Kaur and B. Shiekh, Effects of substituents and charge on the RCHO···X–Y X = Cl, Br, I; Y:-CF3, -CF2H, -CFH2, -CN, -CCH, -CCCN; R:-OH, -OCH3, -NH2, -O-halogen-bonded complexes, *Struct. Chem.*, 2015, 1–11.
74 D. J. R. Duarte, G. L. Sosa, N. M. Peruchena and I. Alkorta, Halogen bonding. The role of the polarizability of the electron-pair donor, *Phys. Chem. Chem. Phys.*, 2016, **18**, 7300–7309.
75 J. Joy, E. D. Jemmis and K. Vidya, Negative hyperconjugation and red-, blue- or zero-shift in X–Z···Y complexes, *Faraday Discuss.*, 2015, **177**, 33–50.

76 J. Joy, A. Jose and E. D. Jemmis, Continuum in the X–Z–Y weak bonds: Z = main group elements, *J. Comput. Chem.*, 2015, **37**, 270–279.
77 I. Alkorta, J. Elguero and J. E. D. Bene, Characterizing Traditional and Chlorine-Shared Halogen Bonds in Complexes of Phosphine Derivatives with ClF and Cl_2, *J. Phys. Chem. A*, 2014, **118**, 4222–4231.
78 A. Bauzá, I. Alkorta, A. Frontera and J. Elguero, On the Reliability of Pure and Hybrid DFT Methods for the Evaluation of Halogen, Chalcogen, and Pnicogen Bonds Involving Anionic and Neutral Electron Donors, *J. Chem. Theory Comput.*, 2013, **9**, 5201–5210.
79 S. J. Grabowski, Hydrogen and halogen bonds are ruled by the same mechanisms, *Phys. Chem. Chem. Phys.*, 2013, **15**, 7249–7259.
80 S. Scheiner, Detailed comparison of the pnicogen bond with chalcogen, halogen, and hydrogen bonds, *Int. J. Quantum Chem.*, 2013, **113**, 1609–1620.
81 Y.-Z. Zheng, N.-N. Wang, Y. Zhou and Z.-W. Yu, Halogen-bond and hydrogen-bond interactions between three benzene derivatives and dimethyl sulphoxide, *Phys. Chem. Chem. Phys.*, 2014, **16**, 6946–6956.
82 C. Wang, L. Guan, D. Danovich, S. Shaik and Y. Mo, The origins of the directionality of noncovalent intermolecular interactions, *J. Comput. Chem.*, 2016, **37**, 34–45.
83 C. Trujillo, G. Sanchez-Sanz, I. Alkorta and J. Elguero, Halogen, chalcogen and pnictogen interactions in $(XNO_2)_2$ homodimers (X = F, Cl, Br, I), *New J. Chem.*, 2015, **39**, 6791–6802.
84 T. Clark, M. Hennemann, J. Murray and P. Politzer, Halogen bonding: the σ-hole, *J. Mol. Model.*, 2007, **13**, 291–296.
85 P. Politzer, J. Murray and M. Concha, Halogen bonding and the design of new materials: organic bromides, chlorides and perhaps even fluorides as donors, *J. Mol. Model.*, 2007, **13**, 643–650.
86 P. Politzer, J. S. Murray and T. Clark, Halogen bonding: an electrostatically-driven highly directional noncovalent interaction, *Phys. Chem. Chem. Phys.*, 2010, **12**, 7748–7757.
87 A. Legon, *Halogen Bonding*, 2008, vol. 126, pp. 17–64.
88 S. V. Rosokha, I. S. Neretin, T. Y. Rosokha, J. Hecht and J. K. Kochi, Charge-transfer character of halogen bonding: Molecular structures and electronic spectroscopy of carbon tetrabromide and bromoform complexes with organic σ- and π-donors, *Heteroat. Chem.*, 2006, **17**, 449–459.
89 Z. Konkoli and D. Cremer, A New Way of Analyzing Vibrational Spectra I. Derivation of Adiabatic Internal Modes, *Int. J. Quantum Chem.*, 1998, **67**, 1–11.
90 D. Cremer, J. A. Larsson and E. Kraka, in *Theoretical and Computational Chemistry, Volume 5, Theoretical Organic Chemistry*, ed. C. Parkanyi, Elsevier, Amsterdam, 1998, pp. 259–327.
91 W. Zou and D. Cremer, Properties of Local Vibrational Modes: The Infrared Intensity, *Theor. Chem. Acc.*, 2014, **133**, 1451.
92 E. B. Wilson, J. C. Decius and P. C. Cross, *Molecular Vibrations. The Theory of Infrared and Raman Vibrational Spectra*, McGraw-Hill, New York, 1955.
93 W. Zou, R. Kalescky, E. Kraka and D. Cremer, Relating Normal Vibrational Modes To Local Vibrational Modes With The Help of an Adiabatic Connection Scheme, *J. Chem. Phys.*, 2012, **137**, 084114.
94 R. Kalescky, W. Zou, E. Kraka and D. Cremer, Local Vibrational Modes of the Water Dimer – Comparison of Theory and Experiment, *Chem. Phys. Lett.*, 2012, **554**, 243–247.
95 M. Freindorf, E. Kraka and D. Cremer, A comprehensive analysis of hydrogen bond interactions based on local vibrational modes, *Int. J. Quantum Chem.*, 2012, **112**, 3174–3187.
96 R. Kalescky, E. Kraka and D. Cremer, Identification of the Strongest Bonds in Chemistry, *J. Phys. Chem. A*, 2013, **117**, 8981–8995.
97 K. Raghavachari, G. W. Trucks, J. A. Pople and M. Head-Gordon, *Chem. Phys. Lett.*, 1989, **157**, 479–483.
98 T. Clark, P. Politzer and J. S. Murray, Correct electrostatic treatment of noncovalent interactions: the importance of polarization, *Wiley Interdiscip. Rev.: Comput. Mol. Sci.*, 2015, **5**, 169–177.
99 P. Politzer, J. S. Murray and T. Clark, Mathematical modeling and Physical Reality in Non-covalent Interactions, *J. Mol. Model.*, 2015, **21**, 52–61.
100 P. Politzer, J. S. Murray and T. Clark, σ-Hole Bonding: A Physical Interpretation, *Top. Curr. Chem.*, 2015, **358**, 19–42.
101 D. Woon and T. J. Dunning, Gaussian Basis Sets for Use in Correlated Molecular Calculations. IV. Calculation of Static Electrical Response Properties, *J. Chem. Phys.*, 1994, **100**, 2975–2988.
102 T. Dunning, Gaussian Basis Sets for Use in Correlated Molecular Calculations. I. The Atoms Boron Through Neon and Hydrogen, *J. Chem. Phys.*, 1989, **90**, 1007–1023.
103 D. Woon and T. Dunning, Gaussian Basis Sets for Use in Correlated Molecular Calculations. III. The Atoms Aluminum Through Argon, *J. Chem. Phys.*, 1993, **98**, 1358–1371.
104 Z. Konkoli and D. Cremer, A New Way of Analyzing Vibrational Spectra III. Characterization of Normal Vibrational Modes in Terms of Internal Vibrational Modes, *Int. J. Quantum Chem.*, 1998, **67**, 29–41.
105 W. Zou and D. Cremer, C_2 in a Box: Determining its Intrinsic Bond Strength for the $X^1\Sigma_g^+$ Ground State, *Chem. – Eur. J.*, 2016, **22**, 4087–4099.
106 E. Kraka, J. A. Larsson and D. Cremer, *Generalization of the Badger Rule Based on the Use of Adiabatic Vibrational Modes in Vibrational Modes in Computational IR Spectroscopy*, Wiley, New York, 2010, pp. 105–149.
107 S. Boys and F. Bernardi, The Calculation of Small Molecular Interactions by The Differences of Separate Total Energies. Some Procedures with Reduced Errors, *Mol. Phys.*, 1970, **19**, 553–566.
108 F. Weinhold and C. R. Landis, *Valency and Bonding: A Natural Bond Orbital Donor – Acceptor Perspective*, Cambridge Uuniversity Press, Cambridge, UK, 2003.
109 D. Cremer and E. Kraka, A Description of the Chemical Bond in Terms of Local Properties of Electron Density and Energy, *Croat. Chem. Acta*, 1984, **57**, 1259–1281.

110 D. Cremer and E. Kraka, Chemical Bonds without Bonding Electron Density – Does the Difference Electron Density Analysis Suffice for a Description of the Chemical Bond?, *Angew. Chem., Int. Ed. Engl.*, 1984, **23**, 627–628.
111 E. Kraka and D. Cremer, in *Theoretical Models of Chemical Bonding. The Concept of the Chemical Bond*, ed. Z. Maksic, Springer Verlag, Heidelberg, Germany, 1990, vol. 2, pp. 453–542.
112 E. Kraka, W. Zou, M. Filatov, J. Grafenstein, D. Izotov, J. Gauss, Y. He, A. Wu, Z. Konkoli and V. Polo, *et al.*, *COLOGNE2016*, 2014; see http://www.smu.edu/catco.
113 J. F. Stanton, J. Gauss, M. E. Harding and P. G. Szalay, *et al.*, *CFOUR, A Quantum Chemical Program Package*. 2010, see http://www.cfour.de.
114 T. Keith, *TK Gristmill Software*, Overland Park KS, USA, 2011, aim.tkgristmill.com.
115 W. Zou, D. Nori-Shargh and J. E. Boggs, On the Covalent Character of Rare Gas Bonding Interactions: A New Kind of Weak Interaction, *J. Phys. Chem. A*, 2013, **117**, 207–212.
116 T. Lu and F. Chen, Multiwfn: A Multifunctional Wavefunction Analyzer, *J. Comput. Chem.*, 2012, **33**, 580–592.
117 D. Setiawan, E. Kraka and D. Cremer, Description of pnicogen bonding with the help of vibrational spectroscopy – the missing link between theory and experiment, *Chem. Phys. Lett.*, 2014, **614**, 136–142.
118 D. Setiawan, E. Kraka and D. Cremer, Strength of the Pnicogen Bond in Complexes Involving Group Va Elements N, P, and As, *J. Phys. Chem. A*, 2014, **119**, 1642–16562.
119 E. Kraka, W. Zou, M. Freindorf and D. Cremer, Energetics and Mechanism of the Hydrogenation of XH_n for Group IV to Group VII Elements X, *J. Chem. Theory Comput.*, 2012, **8**, 4931–4943.
120 R. Kalescky, E. Kraka and D. Cremer, Description of Aromaticity with the help of Vibrational Spectroscopy: Anthracene and Phenanthrene, *J. Phys. Chem. A*, 2014, **118**, 223–237.
121 W. W. Porterfield, *Inorganic Chemistry, A Unified Approach*, Academic Press, San Diego, 1993.
122 R. M. Badger, A Relation Between Internuclear Distances and Bond Force Constants, *J. Chem. Phys.*, 1934, **2**, 128–131.
123 K. Ruedenberg, The Physical Nature of the Chemical Bond, *Rev. Mod. Phys.*, 1962, **34**, 326–352.
124 K. Ruedenberg, in *Localization and Delocalization in Quantum Chemistry*, ed. O. Chalvet, R. Daudel, S. Diner and J. P. Malrieu, Reidel, Dordrecht, Netherlands, 1975, vol. I, pp. 223–245.

